JACS
JOURNAL OF THE AMERICAN CHEMICAL SOCIETY
Communication
pubs.acs.org/JACS

Structural Ordering and Charge Variation Induced by Cation Substitution in (Sr,Ca)AlSiN$_3$:Eu Phosphor

Yi-Ting Tsai,[†] Chang-Yang Chiang,[‡] Wuzong Zhou,[‡] Jyh-Fu Lee,[§] Hwo-Shuenn Sheu,[§] and Ru-Shi Liu*[,†,∥]

[†]Department of Chemistry, National Taiwan University, Taipei 106, Taiwan
[‡]EaStCHEM, School of Chemistry, University of St Andrews, St Andrews, KY16 9ST, United Kingdom
[§]National Synchrotron Radiation Research Center, Hsinchu 300, Taiwan
[∥]Department of Mechanical Engineering and Graduate Institute of Manufacturing Technology, National Taipei University of Technology, Taipei 106, Taiwan

Supporting Information

ABSTRACT: Nitride phosphors are suitable for white light-emitting diode applications. In this study, the structure of phosphor has been modified through cation substitution to induce charge variation and a rearrangement of neighboring nitride clusters, and consequently enhance its luminescent behavior. Substitution of Ca^{2+} by Sr^{2+} cations expanded the lattice volume and the *bc* plane, but shortened the distance between the layers along the *a* axis. Lattice distortion of the framework introduced high-coordination sites in the Sr/Eu centers and adequate space, thereby facilitating charge variation of activators under reduced atmosphere, as detected through X-ray absorption near-edge structure spectroscopy. As such, the photoluminescent intensity of the phosphors increased by more than 10% and a blue shift occurred. The microstructures of the samples were also analyzed using high-resolution transmission electron microscopy. Cation substitution induced a special change in the anion environment, as indicated in the solid-state Raman spectra. Moreover, typical ordering variations in the SiN_4 and AlN_4 clusters are generated in the lattice. Meanwhile, neighbor sequence of $(Si/Al)N_4$ around the divalent centers were observed through solid-state nuclear magnetic resonance spectroscopy. The modified ordering distribution resulted in a rigid structure and improved the thermal quenching behavior. Thermal stability has been enhanced by 10% at 473 K when x = 0.9 in $Sr_xCa_{0.993-x}AlSiN_3:Eu^{2+}_{0.007}$ compared with that at x = 0. This study promotes the research of neighbor sequence for selective tetrahedral sites such as Li, Mg, Al, and Si coordinated by N atoms in contact with cation sites.

Red-emitting phosphor materials have been extensively developed to increase color rendering index and stability in white light-emitting diodes (LEDs).[1−6] Nitridosilicate phosphors, such as $M_2Si_5N_8:Eu^{2+}$ (M = Ca, Sr, and Ba) and $MAlSiN_3:Eu^{2+}$ (M = Ca and Sr), exhibit high chemical and thermal stabilities because of their rigid structures.[7−11] Sr-doped $CaAlSiN_3:Eu^{2+}$ has been synthesized with alloy precursors in a hot isostatic pressing equipment under high pressure and then analyzed for structural properties.[12−15] Nevertheless, the relationship between the structures and luminescent properties of phosphor materials has been rarely discussed. In the present study, disordering of Si/Al in the clusters of $(Si/Al)N_4$ is introduced in the framework through cation substitution to induce charge variation from Eu^{3+} to Eu^{2+}, and simultaneously improves the thermal stability and luminescent properties of the phosphor.

Figure 1 shows the synchrotron X-ray diffraction (XRD) patterns of $Sr_xCa_{0.993-x}AlSiN_3:Eu^{2+}_{0.007}$, which are nearly pure

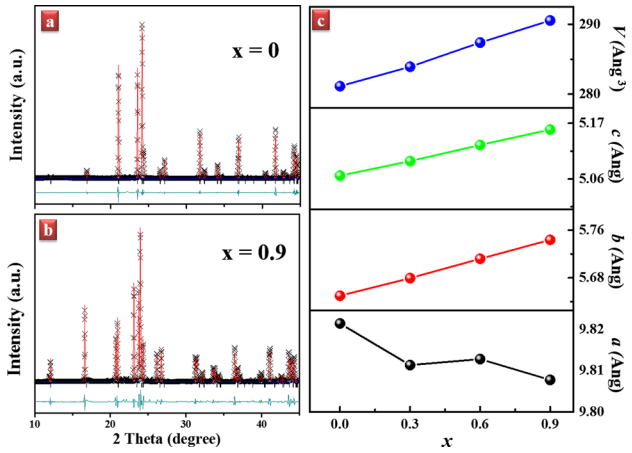

Figure 1. Variations in the lattice parameters (in Å) and volumes (in Å^3) with the corresponding x values in $Sr_xCa_{0.993-x}AlSiN_3:Eu^{2+}_{0.007}$ (x = 0 to 0.9) through Rietveld refinements.

phases of solid solution after Sr doping into the Ca sites. The peaks shift to lower scattering angles because the ionic radius of Sr^{2+} (1.12 Å) is larger than Ca^{2+} (0.99 Å).[16] These results demonstrate that $Sr_xCa_{0.993-x}AlSiN_3:Eu^{2+}_{0.007}$ has an orthorhombic structure with a space group close to $Cmc2_1$. In addition, the lattice parameters *b*, *c*, and *V* present a linear shift because of volume expansion by Sr doping. The unit cell parameters of $Sr_xCa_{0.993-x}AlSiN_3:Eu^{2+}_{0.007}$ from synchrotron X-ray Rietveld

Received: June 11, 2015
Published: July 10, 2015

DOI: 10.1021/jacs.5b06080
J. Am. Chem. Soc. 2015, 137, 8936−8939

refinement are shown in Table S1. The length of the *a* axis shortens when Sr is initially added, maintains constant in a range of $x = 0.3$ to 0.6, and then decreases again with further increasing the Sr concentration. In the solid solution, Sr cations become closer to the second nearest N in comparison with Ca because the Sr cations are larger in size. The distance between the Sr sites and the second nearest coordination site alters the $(Si/Al)N_4$ tetrahedral framework and constricts the second coordination layer. The irregular length along the *a* axis caused by Sr occupancy can be resolved by regulating the bonds and geometries parallel to the *a* axis, the distortion of the $(Si/Al)N_4$ tetrahedral structure, and the decrease in the Sr−N distances in the second nearest coordination site.[12] In the Sr-rich phase, the Sr sites are surrounded by 10 nitrogen atoms, thereby forming a 10-coordinated site. The second nearest coordination distance shortens as Sr occupancy increases, which indicates the presence of a strong interlayer interaction. In particular, expansion of the *bc* plane was investigated using the average Ca−N bond distance (from $d_{Ca-N} = 2.50$ to 2.56 Å calculated from the X-ray Rietveld refinement) within the range of $x = 0.3$ (30% by Sr occupancy) to $x = 0.6$ (60% by Sr occupancy). The average Ca−N bond distance along the *a*-axis remains at $d_{Ca-N} = 2.89$ Å.

X-ray absorption near-edge structure (XANES) spectroscopy was performed to determine the charge variation of Eu in $Sr_xCa_{0.993-x}AlSiN_3:Eu^{2+}_{0.007}$. XANES defines the ionization threshold to the states around the $Eu^{2+}(4f^7)$ and $Eu^{3+}(4f^6)$ absorption edge at 10 eV, and the results are shown in Figure 2a.

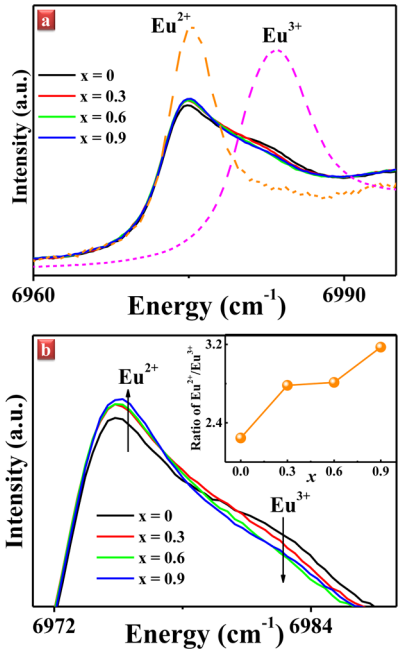

Figure 2. (a) Eu L_3-edge XANES spectra of $Sr_xCa_{0.993-x}AlSiN_3:Eu^{2+}_{0.007}$ ($x = 0$ to 0.9). (b) Dependence of Eu^{2+}/Eu^{3+} within the range of 6970 to 6990 cm^{-1}; the relative intensity of Eu^{2+}/Eu^{3+} is shown in the inset.

The references of the two Eu valence states, namely, Eu^{2+} and Eu^{3+}, are $BaMgAl_{10}O_{17}:Eu^{2+}$ (orange line) and Eu_2O_3 (purple line), respectively. The Eu L_3-edge XANES spectra of the studied $Sr_xCa_{0.993-x}AlSiN_3:Eu^{2+}_{0.007}$ reveal two peaks at 6974 and 6984 eV of Eu^{2+} and Eu^{3+}, respectively. The electron transition of Eu is $2p_{3/2} \rightarrow 5d$. These results indicate that Eu^{2+} and Eu^{3+} coexist in $Sr_xCa_{0.993-x}AlSiN_3:Eu^{2+}_{0.007}$.

Sr^{2+} doping increases the relative intensities of Eu^{2+} absorption at 6974 eV but reduces that of Eu^{3+} at 6984 eV, as shown in Figure 2b. The radii of Eu^{2+} ($r = 1.14$ Å) and Eu^{3+} ($r = 0.95$ Å) are similar to those of Sr^{2+} ($r = 1.12$ Å) and Ca^{2+} ($r = 0.99$ Å), respectively.[16] Therefore, the Sr-rich environment allows Eu^{2+} to easily enter into $Sr_xCa_{0.993-x}AlSiN_3:Eu^{2+}_{0.007}$. The amount of Eu^{3+} decreases with partially transferring to Eu^{2+}. The ratio of Eu^{2+}/Eu^{3+} is shown in the inset of Figure 2b. Consistent with the XRD refinement results, the proportion of Eu^{2+}/Eu^{3+} is similar in a compositional range of $x = 0.3$ to 0.6, which demonstrates the correlation between the *a* axis and the valence state of Eu. In this relationship, the interlayer interaction along the *a* axis directly affects the charge variation of Eu. Eu^{2+} cations prefer the 10-coordinated sites because the closed *a* axis interlayer is connected to the second nearest N atoms in the Sr-rich environment. The local structural schematic graph in Figure 3 presents the charge

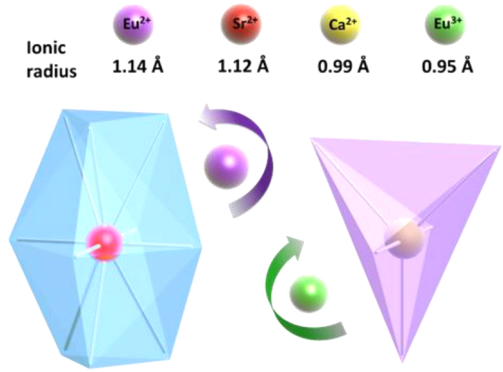

Figure 3. Schematic drawing of local structures. The charge variation of Eu^{3+} activators at the selected Ca^{2+} sites and Eu^{2+} at the Sr^{2+} sites is the proposed mechanism for cation substitution.

variation mechanism. In the Ca-rich environment, it is preferred to form 5-coordination sites, and Ca^{2+} can be replaced by Eu^{3+} because of their similar ionic radii. In the Sr-rich environment, the large space is transformed to 10-coordination sites, thereby causing Eu^{3+} to easily reduce to Eu^{2+} under reduced atmosphere.

The microstructures of the samples were characterized. The powdered sample was deposited on a copper grid coated with a holey carbon film prior to transmission electron microscopy (TEM) and high-resolution TEM (HRTEM) analyses. The selected area electron diffraction patterns (Figure S1) and energy dispersive spectrometry results (Figure S2) show that most of these particles are single crystals, with an element ratio similar to the nominal composition. The HRTEM images show that fine crystalline particles contain several types of defects. Based on the results, the domain structure is the most common defect in all the samples. Other defects, such as antiphase defects, symmetry variation, and layered defects, were observed in samples containing Sr and Ca, as shown in Figure 4.

The domain structures observed in all the samples may be attributed to uneven element distribution. The orthorhombic structure of $CaAlSiN_3$ is a distorted hexagonal wurtzite (AlN), in which some parts of the Al sites are occupied by Ca and Si. Under the optimal condition, 1/3 of the Al sites are occupied by Ca and the other 1/3 occupied by Si. However, if the composition changes within a small area, some defects may form because of atomic dislocation. A similar phenomenon could occur when Sr and Eu are unevenly replaced by Ca. As the radius of Ca^{2+} differs from that of the other two cations, Ca substitution does not only alter the unit cell structure but also forms defects.

DOI: 10.1021/jacs.5b06080
J. Am. Chem. Soc. 2015, 137, 8936−8939

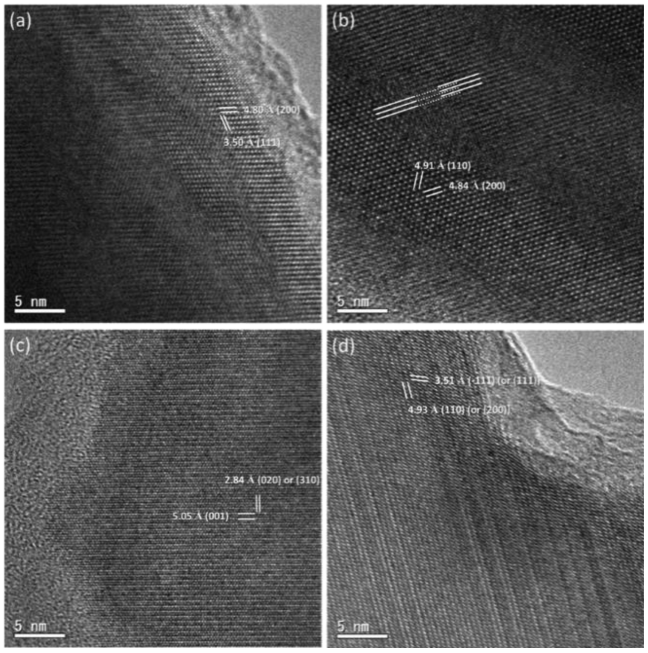

Figure 4. (a) Domain structure in $Ca_{0.993}AlSiN_3:Eu^{2+}_{0.007}$. (b) Antiphase domain (marked by three parallel lines with a shift in the adjacent domain) in $Sr_{0.6}Ca_{0.393}AlSiN_3:Eu^{2+}_{0.007}$. (c) Shortest period of (001) in the image contrast pattern in $Sr_{0.9}Ca_{0.093}AlSiN_3:Eu^{2+}_{0.007}$, which is systematically absent in the parent structure. (d) Layered defects in $Sr_{0.9}Ca_{0.093}AlSiN_3:Eu^{2+}_{0.007}$. Atomic fringes are indexed to the (110) and (−111) or (200) and (111) planes.

Defects seem to be more complicated in Sr-containing samples, namely, $Sr_xCa_{0.993-x}AlSiN_3:Eu_{0.007}$ (x = 0.3, 0.6, and 0.9), compared with those in Sr-free samples. The forbidden diffraction peak of (001) is observed in Sr-containing samples, which implies that the symmetry of the structures is possibly affected by lattice distortion. Antiphase domains are also detected in Sr-containing samples. Layered defects easily occur in samples containing high amounts of Sr; these defects show a disordering along the [200] zone axis or the [110] direction. Meanwhile, atomic arrangements are similar between the Sr-containing and Sr-free samples.

Structural ordering in phosphor lattice is interesting research because of the stability and rigid structure. In previous study, Al^{3+} and Si^{4+} ions could not be separated in the $(Si/Al)N_4$ sites because of disordered distribution. The Raman spectrum of $Sr_xCa_{0.993-x}AlSiN_3:Eu^{2+}$ shown in Figure 5a presents peaks at 400 to 200 cm^{-1}, which represent the rotation and translation interactions between the divalent site and the $(Si/Al)_4$ tetrahedral framework. High-symmetry coordination sites in the Sr center generate different rotation and translation interaction energies compared with that in the Ca center. A broad peak around 350 to 250 cm^{-1} is observed in pure Ca^{2+} sample. Similarly, the effect from the divalent site to the tetrahedral surrounding of $(Si/Al)_4$ is observed because of disordered distribution. As the Sr cations are doped in the phosphor lattice, two sharp peaks are distinctly formed at 292 and 240 cm^{-1}. Hence, the tetrahedral sites of SiN_4 exhibit fast rotation energy and high Raman shifts because Si^{4+} ($^{[4]}r$ = 0.26 Å) is smaller than Al^{3+} ($^{[4]}r$ = 0.39 Å).[17] As such, the distinguished SiN_4 and AlN_4 clusters are confirmed through solid-state Raman studies. Gradual increase of the Sr cations in the structure establishes high coordination centers and compresses the layer of the second sphere. The mechanism of cluster rearrangement

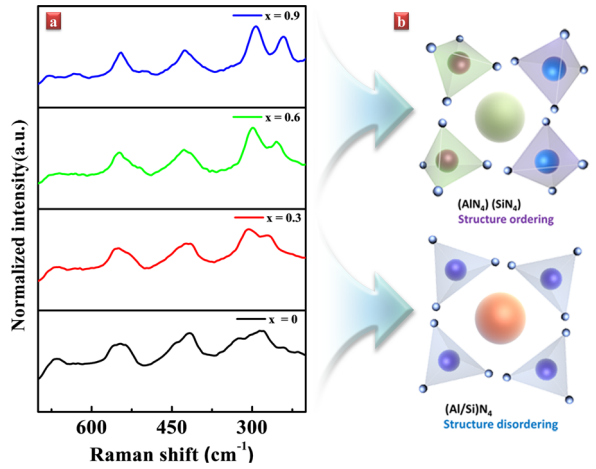

Figure 5. (a) Raman spectrum of $Sr_xCa_{0.993-x}AlSiN_3:Eu^{2+}$ (x = 0, 0.3, 0.6, and 0.9). (b) Schematic graph of separate clusters in the lattice.

from x = 0.3 to 0.6 is proposed. Analogous covalent clusters aggregated in the same side, and the framework distorted to the geometries parallel to the a-axis layers progressively. Rearrangement of the SiN_4 and AlN_4 clusters generated defective and distorted structures. A schematic graph of the separated clusters in the local structure is shown in Figure 5b. Similarly, solid-state NMR spectra demonstrate a downfield peak around 100 ppm (Figure S3). The chemical shift of Al^{3+} cations tends to be relatively downfield with the clustering of the surrounding environment with AlN_4. Hence, peaks at 113 and 102 ppm are assigned to the Al-cluster and Si/Al-equivalent signals, respectively.[18] In addition, Al^{3+} presents limited electron density shielding around the core because of the deshielded environment. This AlN_4 cluster peak confirms that the $(Al/Si)N_4$ environment is separated into the AlN_4 and SiN_4 clusters. These results will improve the selectivity of tetrahedral sites.

Ordering of the homogeneous clusters and activator charges are important factors that affect luminescent properties. Luminescence intensity and thermal quenching behavior are the primary focus in research for LED applications. The content of Eu^{2+} is the major activator in $Sr_xCa_{0.993-x}AlSiN_3:Eu^{2+}_{0.007}$ for blue and UV-LED phosphor applications because of the typically strong and wide-band luminescence of the 4f−5d transition under excitation wavelengths from near UV to the blue region.[19] Figure 6a shows the excitation spectra from 325 to 540 nm and the specific emission spectra under 460 nm. The deep red peak located at 650 nm in $Ca_{0.993}AlSiN_3:Eu^{2+}_{0.007}$ is a typical case, and Sr-doped samples exhibits a blue shift to 619 nm when x = 0.9. The photoluminescence emission spectra reveal a conventional blue shift when the divalent cation changes from Ca to Sr because the Sr site is larger than the Ca site, which results in reduced crystal-field splitting strength. The emission spectra further show that luminescence intensity is enhanced by Sr doping, with more than 10% for the emission intensity and 5% for the external quantum efficiency increase at x = 0.9, compared with that in the parent sample. The overall trend observed in emission intensity corresponds with the structure and valence state of Eu. Temperature-dependent emission spectra determined from 298 to 573 K with the fitting equation $I_T/I_0 = [1 + D\exp(-E_a/kT)]^{-1}$ are shown in Figure 6b. A systematic increase in thermal stability is observed in $Sr_xCa_{0.993-x}AlSiN_3:Eu^{2+}_{0.007}$, with approximately 10% increase in thermal stability at 473 K (working temperature of high power LED devices). Eu^{3+} is not

DOI: 10.1021/jacs.5b06080
J. Am. Chem. Soc. 2015, 137, 8936−8939

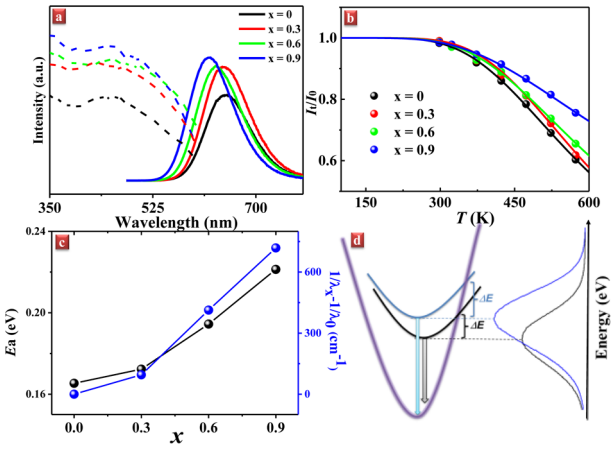

Figure 6. (a) Excitation (dashed lines) and emission (solid lines) spectra of $Ca_{0.993-x}Sr_xAlSiN_3:Eu^{2+}$ (x = 0, 0.3, 0.6, and 0.9). (b) Temperature-dependent emission intensity fitting curve and (c) related tendencies of activation energy (in eV) and emission blue-shift energy (in cm^{-1}). (d) Schematic graph with energy in the x-axis; x = 0 (black line) and x = 0.9 (blue line).

the major emission center in this phosphor. If Eu^{3+} concentration increased, luminescence intensity would be decreased due to the f−f transition, as luminescence "killer". Activation energy represents the quenching process of the lowest vibrational energy level to the crossing points of the ground and excited states. The similar tendencies of activation and blue-shift energies and the schematic graph with energy as the x-axis are shown in Figure 6c,d, respectively. Volume expansion of the lattice reduces the crystal-field splitting energy when the state energy gap increases between the energy levels at the excited and ground states.

Structural studies of ordering is a novel research field.[20,21] The ordering effect would create a rigid structure and reduce energy loss caused by heat vibration in a lattice. In the present study, a homogeneous ordering of SiN_4 and AlN_4 is introduced through cation substitution. The relationship between the thermal quenching behavior and ordering measurement indirectly confirms that ordering is a factor that controls thermal stability. A method is also proposed to optimize the parameters required for phosphor applications.

In summary, homogeneous ordering and charge variation of activators were investigated through solid-state techniques. Enhanced-luminescence intensity and thermal properties in $Sr_xCa_{0.993-x}AlSiN_3:Eu^{2+}$ were also simultaneously studied. The local structures of different coordination sites influence the layer in lattice, thereby inducing charge variation and generating responses vital for luminescent properties. An ordering of the AlN_4 and SiN_4 clusters is obtained and improved substitutability of tetrahedral environment. These results do not only confirm the local structure through a subtle analysis technology but also improve phosphor properties for LEDs applications.

■ ASSOCIATED CONTENT

Supporting Information

Experimental methods and supporting tables and figures. The Supporting Information is available free of charge on the ACS Publications website at DOI: 10.1021/jacs.5b06080.

■ AUTHOR INFORMATION

Corresponding Author

*rsliu@ntu.edu.tw

Notes

The authors declare no competing financial interest.

■ ACKNOWLEDGMENTS

This work was supported by the Ministry of Science and Technology of Taiwan (Contract No. MOST 101-2113-M-002-014-MY3) and Mitsubishi Chemical Group, Science and Technology Research Center Inc., Japan. We also appreciate to the discussion by Dr. Kyota Ueda and Mr. Fumitaka Yoshimura.

■ REFERENCES

(1) Xie, R. J.; Hirosaki, N. *Sci. Technol. Adv. Mater.* **2007**, *8*, 588.
(2) Wang, S. S.; Chen, W. T.; Li, Y.; Wang, J.; Sheu, H. S.; Liu, R. S. *J. Am. Chem. Soc.* **2013**, *135*, 12504−12507.
(3) Uheda, K.; Hirosaki, N.; Yamamoto, Y.; Naito, A.; Nakajima, T.; Yamamoto, H. *Electrochem. Solid-State Lett.* **2006**, *9*, H22.
(4) Chen, W. T.; Sheu, H. S.; Liu, R. S.; Attfield, J. P. *J. Am. Chem. Soc.* **2012**, *134*, 8022.
(5) Höppe, H. A. *Angew. Chem., Int. Ed.* **2009**, *48*, 3572.
(6) Xie, R. J.; Hirosaki, N.; Li, Y.; Takeda, T. *Materials* **2010**, *3*, 3777.
(7) Yeh, C. W.; Chen, W. T.; Liu, R. S.; Hu, S. F.; Sheu, H. S.; Chen, J. M.; Hintzen, H. T. *J. Am. Chem. Soc.* **2012**, *134*, 14108.
(8) Uheda, K.; Hirosaki, N.; Yamamoto, H. *Phys. Status Solidi A* **2006**, *203*, 2712.
(9) Mikami, M.; Uheda, K.; Kijima, N. *Phys. Status Solidi A* **2006**, *203*, 2705.
(10) Mikami, M. *ECS J. Solid State Sci. Technol.* **2013**, *2*, R3048.
(11) Huang, W. Y.; Yoshimura, F.; Ueda, K.; Pang, W. K.; Su, B. J.; Jang, L. Y.; Chiang, C. Y.; Zhou, W. Z.; Nguyen, H. D.; Liu, R. S. *Inorg. Chem.* **2014**, *53*, 12822.
(12) Kim, Y. S.; Choi, S. W.; Park, J. H.; Bok, E.; Kim, B. K.; Hong, S. H. *ECS J. Solid State Sci. Technol.* **2013**, *2*, R3021.
(13) Watanabe, H.; Kijima, N. *J. Alloys Compd.* **2009**, *475*, 434.
(14) Watanabe, H.; Wada, H.; Seki, K.; Itou, M.; Kijima, N. *J. Electrochem. Soc.* **2008**, *155*, F31.
(15) Watanabe, H.; Yamane, H.; Kijima, N. *J. Solid State Chem.* **2008**, *181*, 1848.
(16) Shannon, R. D. *Acta Crystallogr., Sect. A: Cryst. Phys., Diffr., Theor. Gen. Crystallogr.* **1976**, *A32*, 751.
(17) Wu, Y. F.; Chan, Y. H.; Nien, Y. T.; Chen, I. G. *J. Am. Ceram. Soc.* **2013**, *96*, 234.
(18) Fitzgerald, J. J. *Solid-State NMR Spectroscopy of Inorganic Materials*; American Chemical Society: Washington, D.C., 1999.
(19) Shigeo, S.; William, M. *Phosphor Handbook*; CRC Press: Washington, D.C., 1998.
(20) Pust, P.; Wochnik, A. S.; Baumann, E.; Schmidt, P. J.; Wiechert, D.; Scheu, C.; Schnick, W. *Chem. Mater.* **2014**, *26*, 3544.
(21) Pust, P.; Weiler, V.; Hecht, C.; Tücks, A.; Wochnik, A. S.; Henß, A.-K.; Wiechert, D.; Scheu, C.; Schmidt, P. J.; Schnick, W. *Nat. Mater.* **2014**, *13*, 891.

DOI: 10.1021/jacs.5b06080
J. Am. Chem. Soc. 2015, 137, 8936−8939